Nano Research

Open Access

Research Article

Solvent-resistant polyHOF membranes with well-defined nanostructures and high structural stability

Jiaojiao Duan[1], Xuan Wang[1], Weiliang Li[1], Jingjing Chen[1], Ruilong Li[2], Xiaoli Wu[2], Yanan Liu[3], Yifan Li[1] ✉, Wenjia Wu[1], and Jingtao Wang[1] ✉

[1] School of Chemical Engineering, Zhengzhou University, Zhengzhou 450001, China
[2] Henan Institute of Advanced Technology, Zhengzhou University, Zhengzhou 450003, China
[3] School of Chemical Engineering and Technology, Collaborative Innovation Center of Ecological Civilization, Hainan University, Haikou 570228, China

Cite this article: *Nano Research*, **2025**, *18*, 94907406. https://doi.org/10.26599/NR.2025.94907406

ABSTRACT: Hydrogen-bonded organic frameworks (HOFs) have gained growing attention in the design and fabrication of advanced nanoporous membranes, while there have been few reports about their potential applications requiring long-term immersion of membranes in liquid, especially organic solvents. Herein, we fabricated solvent-resistant HOF@polymer (polyHOF) membranes through facile polymer network-reinforced synthesis strategy of polyHOF nanosheets, followed by vacuum filtration. Two hydrophilic polymers, polyvinyl alcohol (PVA) and polyethylene glycol (PEG), were selected to form multiple-site hydrogen bonding interactions with the pristine HOF framework. Benefiting from the reinforced hydrogen bonding networks and the electrostatic interactions between polymer chains and the HOF framework, these polyHOF membranes demonstrate exceptional stability in many solvents (even in water) for more than 30 days. Moreover, the enriched and regular channel of HOF enables the ultrafast solvent permeance (367.8 $L \cdot m^{-2} \cdot h^{-1} \cdot bar^{-1}$ to water) and precise molecular sieving (> 99.6% rejection to Evans blue). This modification technique presents a generic and promising strategy to robust HOF membranes, which can maintain high performance during long-term operation.

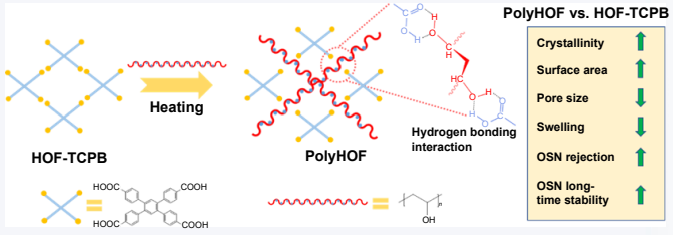

KEYWORDS: hydrogen-bonded organic frameworks, organic solvent nanofiltration, lamellar membrane, poly(vinyl alcohol), stability

1 Introduction

The extensive utilization of organic solvents in daily chemical production has rendered the separation and extraction of high value-added substances from organic waste liquids as the main process [1, 2]. Distinguished from traditional thermal-driven distillation and crystallization, pressure-driven membrane separation technologies, especially organic solvent nanofiltration (OSN), have been widely employed to separate small molecules, such as inorganic salts, amino acids, and dyes [3–5]. Polymer membranes are closer to practical applications due to their low cost and ease of processing, while the essential requirement of a low swelling degree in solvent—arising from the concerns on membrane selectivity and stability—restricts their permeance [6]. For the purpose of integrating high permeance and stability, nanoporous materials, including zeolites, metal–organic frameworks (MOFs), covalent organic frameworks (COFs), and porous organic polymers (POPs), have been considered as promising materials for membrane separation and extensively investigated over the last two decades [7–11]. These porous frameworks composed of different organic linkers or inorganic linkers can construct rigid and stable frameworks with abundant transfer channels in the membrane, thus providing great opportunities for overcoming the shortcomings of polymer membranes. However, the brittleness of these molecular sieving materials and the difficulty in controlling non-selective defects for large-area membranes retard their steps toward industrial applications [12].

Hydrogen-bonded organic frameworks (HOFs) materials are an emerging class of functional porous crystalline materials, which are assembled by small organic molecules mainly through hydrogen

Received: February 14, 2025; **Revised:** March 24, 2025
Accepted: March 26, 2025

✉Address correspondence to Yifan Li, yf_li@zzu.edu.cn; Jingtao Wang, jingtaowang@zzu.edu.cn

bonding [13–15]. Apart from the common benefits of framework materials, HOFs possess unique advantages, such as mild synthesis conditions, adaptive structural transformations, and good solution processability, owing to the relatively weak link between monomers [16]. These features render HOFs highly attractive candidates for addressing the membrane-forming issues of framework materials at low cost. The reversible hydrogen bonding allows re-arrangement of undesired structures so as to eliminate defects, and the all-organic constitution is intrinsically compatible with flexible and organic materials, which are often adopted to facilitate large-area membrane fabrication [17]. Nevertheless, HOFs are thought to suffer from instability, reflecting the other side of the weak inter-monomer linkage. The attention focused on the stability of HOFs is not adequate to support the substantial development of new functional HOF materials for applications in membranes and other fields.

The HOF with hydrogen bonding system has a remarkably flexible nature that ensures thermodynamic equilibrium and facilitates easy processing into membranes. As a result, the use of this remarkable crystalline material in the manufacture of high-quality membranes is more designable and predictable. Various preparation methods for HOF-based membranes, including solution processing [18], electrophoretic deposition [19, 20], solvent casting [21, 22], vacuum filtration [23], and so on. Due to the reversible hydrogen bonds, HOFs are able to dissolve in organic solvents [24]. This characteristic allows HOFs to be processed into membranes via a solution-processing route similar to that of polymers, which facilitates easier scale-up compared to the conventional solvothermal synthesis of polycrystalline membranes. Li et al. reported a novel HOF-based mixed matrix membranes (MMMs) via blending HOF-30 into polyimide (PI) matrix for gas separation. The HOF-30@PI MMMs showed excellent stability and had no obvious separation performance degradation after 240 h of testing [21]. However, HOFs are mainly employed as fillers to enhance the properties of polymer membrane matrices. It remains a considerable challenge to harness the full potential of the intrinsic high perm-selectivity offered by HOF materials. Li et al. reported the fabrication of macrocycle-based HOFs, mHOF-SYSU101, which achieved a remarkable 99% adsorption of iodine from seawater in just 2 min and maintained fully reversible adsorption capacity over five cycles, showing the opportunity of acquiring stable HOF materials in liquid environment [18]. Despite this advance, the fabrication of HOF membranes for applications in solvents is seldom reported, which is highly related to the concerns about excessive membrane swelling or even dissolution.

With the aid of exploring the availability of HOF membranes in solvents, we designed and fabricated HOF membranes in which the frameworks were reinforced by polymer network strategy. This strategy is believed to combine the advantages of polymer and crystalline HOF, such as excellent chemical stability, high crystallinity, and ordered pore structure [25–27]. Two hydrophilic polymers, polyvinyl alcohol (PVA) and polyethylene glycol (PEG), were selected to form multiple-site hydrogen bonding interactions with the pristine HOF monomers, 1,2,4,5-tetrakis(4-carboxyphenyl)benzene (TCPB). The flexible polymer chain segments that bind to HOF nanosheets could result in tightly stacked nanosheets and thus contribute to the crystallinity and stability of the corresponding lamellar membranes. The reinforced frameworks and well-defined nanochannels of polyHOF membranes allowed ultrafast solvent transport and precise molecular sieving (water permeance 367.8 $L \cdot m^{-2} \cdot h^{-1} \cdot bar^{-1}$ and Evans blue (EB) rejection > 99.6%). The polyHOF membranes demonstrate stable nano/sub-nanometer level selectivity during long-term immersion in both water and organic solvent. This modification technique presents a future-oriented strategy for acquiring adequate stability of HOF membranes under harsh conditions.

2 Experimental

2.1 Materials and chemicals

Organic ligand TCPB was purchased from Jilin Chinese Academy of Sciences-Yanshen Technology Co., Ltd. PEG, PVA, and N,N-dimethyl formamide (DMF) were purchased from Shanghai Maclin Biochemical Technology Co., Ltd. Ethanol, acetonitrile, ethyl acetate, n-hexane, and toluene were obtained from Tianjin Kermel Chemistry Reagent Technology Co., Ltd. Nylon microfiltration substrates with 0.2 μm pore size and 47 mm in diameter were bought from Tianjin Jinteng Experimental Equipment Co., Ltd. Methyl orange (MO), methylene blue (MnB), crystal violet (CV), acid yellow 79 (AY 79), and EB were supplied by Aladdin Biochemical Technology Co., Ltd. Deionized water was used throughout the experiment. All chemicals were used without further purification.

2.2 Preparation of HOF-TCPB and polyHOF membranes

HOF-TCPB nanosheets were synthesised by self-assembly of 1,2,4,5-tetrakis(4-carboxyphenyl) benzene (TCPB) in an aqueous environment according to Ref. [23]. TCPB (55 mg, 0.1 mmol) was dissolved in DMF (7.5 mL) and water (200 mL) mixture solution at room temperature and stirred for 1 h to obtain HOF-TCPB nanosheet colloidal suspension, which was usually stirred for 4 h and centrifuged and dried to collect the nanosheets. Polymer aqueous solution (1 $g \cdot L^{-1}$) was quickly injected into the HOF-TCPB nanosheet solution at 50 °C. After stirring 12 h at room temperature, the HOF@polymer (polyHOF) nanosheets were obtained. The products were separated via centrifugation at 10,000 rpm for 10 min. The optimal polymer content compared to HOF-TCPB nanosheet was investigated and determined to be 30 wt.%. The HOF-TCPB and polyHOF membranes were fabricated by vacuum filtrating the above colloidal suspension of HOF-TCPB and polyHOF nanosheets on a Nylon support substrate, respectively. Subsequently, the obtained membranes were dried in an oven set at a temperature of 60 °C for a period of 2 h in order to facilitate their subsequent utilization.

2.3 Characterizations

The structure and morphology of HOF nanosheets and membranes were characterized by atomic force microscopy (AFM, Bruker Dimension Fast Scan), scanning electron microscopy (SEM, ZEISS Sigma 300), and transmission electron microscopy (TEM, FEI Talos F200S) measurements. The crystallinity of HOF membranes was evaluated via X-ray diffraction (XRD, D8-Focus, Cu-Kα) measurement. Thermogravimetry/differential scanning calorimetry (TG/DSC) simultaneous thermal analysis (TG-DSC, NETZSCH STA 449 F3) of HOF membranes was tested on a thermogravimetric analyzer device from 30 to 800 °C with a heating rate of 10 $°C \cdot min^{-1}$ under flowing N_2 atmosphere. The chemical properties were analyzed by X-ray photoelectron spectroscopy

(XPS, Thermo Scientific K-Alpha) and Fourier transform infrared (FTIR) spectroscopy (Bruker Vertex70) measurements. The chemical structures of HOF lamellar framework membranes were analyzed by proton nuclear magnetic resonance (^{1}H NMR, Bruker 400M) measurement through dissolving them in dimethyl sulfoxide-d6. N_2 sorption measurements were conducted using a Micrometritics ASAP 2460 system. The Brunauer–Emmett–Teller (BET) surface area and pore size distribution were calculated from the N_2 adsorption isotherms. The contact angle was conducted on a Face-Kyowa (FACE, model OCA25) at room temperature to evaluate the hydrophilicity of membranes. The nanoscratch results were measured with Nano Hardness Tester (NANOVEA PB1000), and the type of diamond indenter is nano conical 120° 5 μm.

2.4 Measurement of membrane swelling ratio (S_t (%))

The S_t was tested and obtained from the weight change between a dry membrane and a wet one. Specifically, the pristine membrane was dried in an oven at 60 °C for 2 h with the weight of the pristine mass (M_0 (g)). Subsequently, the swollen sample was taken out and quickly wiped away the excess solvent with air-laid paper, and the weight of the mass of soaking dependent on time (M_t (g)) was measured. The S_t was calculated according to Eq. (1)

$$S_t = \left(1 - \frac{M_t}{M_0}\right) \times 100\% \quad (1)$$

Note, the swelling behavior of the membranes is not always isotropic. It is also meaningful to analyze the swelling by the change in the thickness of the membranes.

2.5 Nanofiltration performance.

The organic solvent and dye solution (10 ppm) was added into the dead-end unit cell to measure the solvent permeance (P ($L{\cdot}m^{-2}{\cdot}h^{-1}{\cdot}bar^{-1}$)) and rejection of membranes, respectively, in a N_2 pressurized cell of 3 bar. Some physical properties of the five dyes are given in Table S1 in the Electronic Supplementary Material (ESM). The P was calculated by Eq. (2)

$$P = \frac{V}{\Delta P A t} \quad (2)$$

where V (L), ΔP (bar), A (m^2), and t (h) are the permeate volume, pressure, effective membrane area, and time, respectively.

The dye rejection performance (R) was calculated by Eq. (3)

$$R = \left(1 - \frac{C_p}{C_f}\right) \times 100\% \quad (3)$$

where C_p and C_f are the concentrations of permeate solution and pristine solution, respectively. The average value of three times was taken as the final value of permeance and dye rejection.

3 Results and discussion

3.1 Fabrication and characterization of HOF nanosheets

As illustrated in Fig. 1(a), HOF-TCPB nanosheets were successfully prepared using the reported method [23]. Subsequently, PVA was introduced to form composite HOF@PVA nanosheets. AFM images (Figs. 1(b) and 1(c)) reveal that the lateral dimensions of the HOF-TCPB and HOF@PVA nanosheets were approximately 1.7 and 2.4 μm, with thickness of 4 nm. As shown in the inset of AFM images, the nanosheet solution exhibits a distinct Tyndall effect, indicating that these nanosheets are uniformly dispersed. Meanwhile, as shown in Fig. S1 in the ESM, with the increase of PVA percentage to TCPB, the average size of nanosheets enlarges continuously (1–3 μm). Furthermore, the TEM images in Figs. 1(e) and 1(f) demonstrate that the crystal structures of the HOF-TCPB and HOF@PVA nanosheets are analogous, exhibiting distinct lattice fringes. To ascertain the applicability of this strategy, we employed PEG as an alternative polymer to prepare polyHOF nanosheets. Figures 1(d) and 1(g) demonstrate that HOF@PEG nanosheets also exhibit a typical two-dimensional (2D) morphology, with thickness and lateral dimensions of approximately 5.0 nm and 2.3 μm, respectively. Furthermore, the HOF@PEG nanosheets exhibit clear lattice fringes. Powder XRD (PXRD) patterns provide information about the crystal structure (Fig. S2 in the ESM). The characteristic peaks of HOF-TCPB nanosheet powders at 6.9°, 13.9°, 18.8°, and 20.2° are attributed to the (110), (220), (221), and (112) crystal planes, respectively, which are associated with the highly crystalline HOF-TCPB structure [28, 29]. The PXRD measurements also show that the obtained polyHOF has the similar PXRD pattern as HOF-TCPB but higher degree of crystallinity than the latter, as supported by TEM images. These results imply that the polymers added did not simply blend with HOF-TCPB nanosheets but led to the formation of new composite frameworks. The driving force that causes the assembly process can be illustrated by the change of surface charges of the nanosheets (Fig. S3 in the ESM).

The zeta potential of the HOF-TCPB nanosheet suspension is about −37.1 mV, indicating that the HOF nanosheets are negatively charged, which could be attributed to the presence of unprotonated carboxyl groups. Whereas, the presence of polymer decreases the negative potential of HOF@PVA nanosheets (−19.3 mV) and HOF@PEG nanosheets (−32.5 mV). The opposite charge of the HOF-TCPB nanosheets and PVA solutions enhances the electrostatic interaction between them. Additionally, hydrogen bonds formed between their functional groups, contributing to their strong binding. The PVA chains caused re-arrangement of the pristine frameworks while maintaining the morphology of nanosheets, which then stacked together to form a stable lamellar membrane structure. The electrostatic interactions observed between the HOF nanosheets and the polymer indicate that the latter plays a non-negligible role in the growth of the former.

3.2 The microstructure of HOF membranes

In this study, polyHOF nanosheets were prepared using the polymer network-reinforced strategy. The preparation of HOF membranes involves the intricate process of combining negatively charged HOF nanosheets with positively charged polymer molecular chains through electrostatic interactions, resulting in the formation of polyHOF nanosheets. Under heating conditions, the adjacent nanosheets were interlocked through the formation of a polymer network. The polymer chains can be firmly anchored in the HOF framework, which avoids polymer loss and meanwhile increases the hydrogen bonding with the HOF framework. HOF membranes could be prepared by filtration of the nanosheets onto a porous support. With the purpose of facilitating membrane characterization, swelling measurement and stability evaluation, we prepared free-standing membranes with a thickness of 10–15 μm (Figs. S4 and S5 in the ESM), slightly greater than that of the HOF separation membranes reported in Refs. [30, 31]. Each membrane exhibits a layered structure comparable to that observed in other

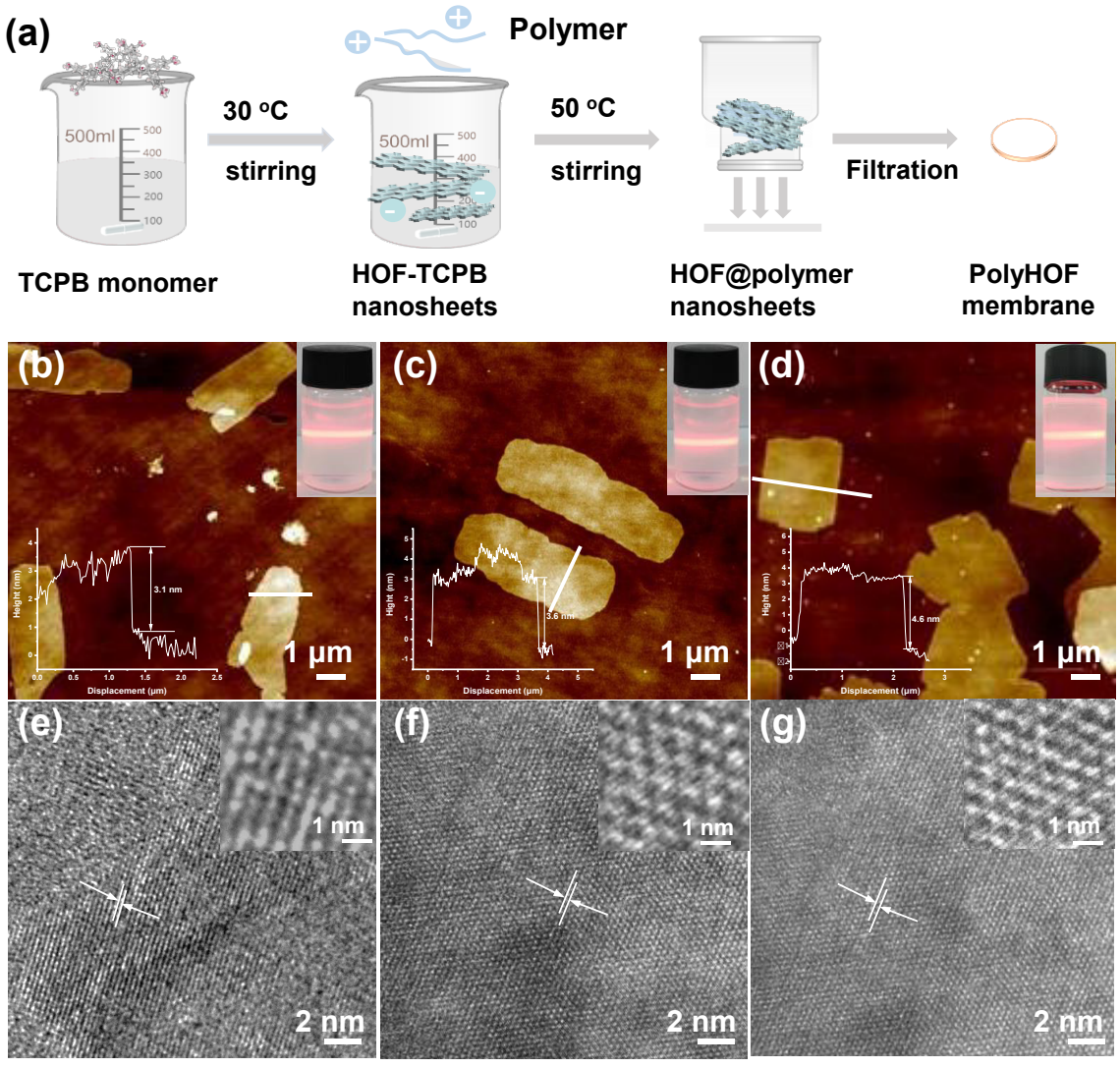

Figure 1 Microstructure of HOF nanosheets. (a) Preparation procession of HOF-TCPB and polyHOF nanosheets. ((b)–(d)) AFM images of HOF-TCPB, HOF@PVA, and HOF@PEG nanosheets (inset: images show the Tyndall effect of HOF nanosheets in water). ((e)–(g)) TEM images of HOF-TCPB, HOF@PVA, and HOF@PEG nanosheets.

2D membranes, such as graphene oxide membranes [32]. Compared to the rough surface of HOF-TCPB membrane, HOF@PEG and HOF@PVA membranes show much smoother membrane surface due to the flexible polymer constitutes. The formation of hydrogen bonds between the oxygen-containing groups of polymer and the excess carboxyl groups of HOF-TCPB nanosheets could also contribute to the eliminating of defects, which could be found on the surface of the pristine HOF-TCPB membrane.

The molecular-level structures of membranes are summarized in Fig. 2. The FTIR spectra in Fig. 2(a) show that the HOF@PEG and HOF@PVA membranes show characteristic bands at 3509 and 3513 cm^{-1}, respectively, corresponding to the stretching vibration of the OH group [33–35]. In addition, it is found that carboxyl group band (1681 cm^{-1}) in HOF-TCPB membrane shifts toward lower wavenumbers (1676 and 1671 cm^{-1} for HOF@PEG and HOF@PVA membranes, respectively). Meanwhile, the intensities of the bands from pure HOF-TCPB membrane gradually decrease with increasing PVA content. The characteristic peaks at 1682 cm^{-1} of PVA shifted to lower wavenumbers (Fig. S6 in the ESM). All of those changes imply the formation of strong intermolecular interactions, including hydrogen bonding and electrostatic attractions, between HOF-TCPB nanosheets and PVA chains [36]. This observation supports the successful synthesis of polyHOF membranes. The Raman results further corroborate the observed alterations in interactions, where the characteristic bands at 1326 cm^{-1} (C–O) and 1624 cm^{-1} (C=C) exhibit enhancement and shifts upon addition of polymer (Fig. S7 in the ESM) [37, 38]. This may be due to the oxygen atom of the inserted polymer being able to form hydrogen bonds with unbonded COOH, shortening the O···H–O distance and enhancing the hydrogen bonds strength. In the ^{1}H NMR results in Fig. S8 in the ESM, the peak intensities at 3.3 ppm are much lower for HOF@PVA and HOF@PEG membranes compared to HOF-TCPB membrane. This indicates that there is more H_2O in HOF-TCPB, suggesting that only some of the carboxyl groups form carboxyl dimers [39]. The strong signal of the proton peak on the main chain of PVA at 7.8 ppm indicates that part of PVA remains rigid and has some interchain hydrogen bonding with HOF-TCPB [40]. The structure of the HOF membranes was characterized using XRD measurement. The peak

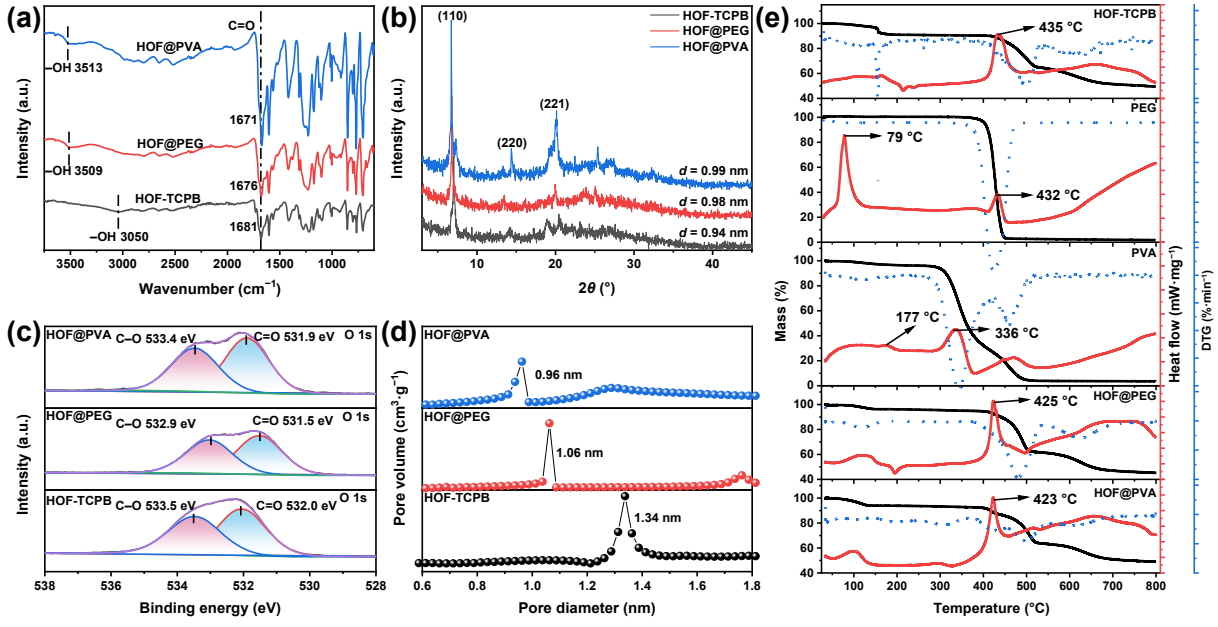

Figure 2 Characterization of HOF lamellar membranes. (a) FTIR spectra, (b) XRD patterns, (c) XPS spectra of O 1s, and (d) pore distributions of different HOF membranes. (e) TG-DSC of polymers and HOF membranes.

at $2\theta = 6.9°$ (refers to (110) plane) reflects the typical topology of the framework, and the three HOF membranes display similar crystalline structures (Fig. 2(b)). The addition of polymer shifts the peak of polyHOF membranes towards a small angle and increases the interlayer spacing, and peak intensity decreases with increasing polymer content (Fig. S9 in the ESM). According to the XPS full spectroscopy and deconvolution in the O 1s and C 1s bands (Fig. 2(c) and Figs. S10 and S11 in the ESM), the O 1s deconvolution peak at 532.0 eV (assigned to O=C) for HOF-TCPB shifts to 531.5 and 531.9 eV for HOF@PEG and HOF@PVA, respectively. Since there is no C=O bond in either PEG or PVA, such shifts clearly illustrate the increase of electron cloud density on the carboxyl group of TCPB, which reflects the effect of hydrogen bond interactions among TCPB monomer and polymer chains. The collective findings indicate the structural integrity of the HOF membrane morphology and the formation of robust frameworks [41–43]. In addition, compared to the pristine HOF-TCPB membrane, a reduction in the average pore size was observed for HOF@PEG and HOF@PVA membranes (from 1.34 to 1.06 and 0.96 nm, respectively, see Fig. 2(d)), which could be explained by the partial overlapping by those "excessive" polymer segments without participating the formation of hydrogen bonds with TCPB monomers. Unexpectedly, an increase in the specific surface area was also observed for HOF@PEG and HOF@PVA membranes (from 57 to 143 and 285 $m^2 \cdot g^{-1}$, respectively, see Fig. S12 in the ESM), consistent with the XRD results demonstrating enhanced crystallinity. It is reasonable to speculate that the decrease of average pore size is caused by well-organized polymer segments rather than random distributed ones.

TG/DSC simultaneous thermal analysis (TG-DSC) was used to further determine the composite structures of the polyHOFs [44]. As can be seen from Fig. 2(e), the thermal degradation temperature of PVA and PEG are determined to be 336 and 432 °C, respectively. The sharp peak at 79 °C was observed for PEG crystalline melting, as well as a weak broad peak at 177 °C for PVA crystalline melting (detailed data are given in Table S2 in the ESM). On the other hand, for HOF@PEG and HOF@PVA, no melting temperature of the polymers was observed, and the thermal degradation temperature values became similar to that of HOF-TCPB and other reported HOFs [45, 46]. In particular, HOF@PVA shows much higher thermal degradation temperature than PVA, hinting that the PVA chains are "inserted" into the HOF-TCPB framework and form a new crystalline phase. These results provide solid evidence that the introduced PVA or PEG induced the re-construction of HOF-TCPB nanosheets and the generation of polyHOF frameworks. Furthermore, according to the nanoscratch results (Fig. S13 in the ESM), HOF@PVA membrane displays a critical load of 23.6 mN, three times higher than that of HOF-TCPB membrane. The PVA-enabled reinforcement of HOF-TCPB membrane could be attributed to the immobilization of covalently linked macromolecules in the pristine crystalline frameworks constructed through only hydrogen bonding. Thanks to the strong hydrogen bonding among TCPB monomer and PVA chains, the covalent connection of PVA units could further contribute to the overall mechanical performance of the composite, rather than suffer from frustrating phase separation [47]. Such reinforcement is, therefore, expected to enhance the membrane stability under harsh conditions.

3.3 Stability of HOF lamellar membranes

To meet the industrial requirements for practical applications, OSN membranes should be stable in different organic solvents. The attentions were first focused on the long-term stability of its colloidal solutions. To assess the stability of the HOF nanosheet, we subjected the colloid solution to an ultrasonication bath for 1 h. All the nanosheet dispersions for stability comparison were stored in open vials at room temperature. The as-obtained HOF colloidal solution exhibited a light milky white color and showed a distinct Tyndall effect. As the storage time was prolonged, the HOF dispersion was observed to remain stable, and the nanosheets within the dispersion did not exhibit any tendency to disintegrate or aggregate (Fig. S14 in the ESM). The structural stability of the HOF membranes was further verified by immersing them in an

ultrasonic bath for 20 min, and no disintegration or dispersion was observed when ultrasonic vibration was applied (Fig. S15 in the ESM), which suggests that the HOF membranes could withstand harsh working conditions.

To investigate the solvent stability of HOF membranes, HOF-TCPB, HOF@PVA, and HOF@PEG membranes were immersed in different solvents. The solvents were selected to cover different chemical structures: an aromatic carbohydrate (toluene), an aliphatic carbohydrate (n-hexane), an ester (ethyl acetate), and a nitrile (acetonitrile). This is useful to gain a qualitative insight into the interaction mechanisms between different solvents and membranes. All solvents used were of analytical grade. Some physical properties of the four organic solvents and water are given in Table S3 in the ESM. Each sheet of the three membrane types was then exposed to one of the following solvents for 30 days: n-hexane, toluene, ethyl acetate, acetonitrile, and water. This was done by immersing the membrane sheets in Petri dishes that were filled with the respective solvents and refilled daily so that the membranes never became dry due to the evaporation of the solvents. An exposure time of 30 days was chosen because no additional visual damage was observed after this period in preliminary experiments with each of the solvents. After solvent exposure, the membranes were again examined visually and microscopically by SEM measurement. Finally, pure water flux and dye rejection were measured under the same conditions. The swelling of three HOF membranes in n-hexane, toluene, ethyl acetate, acetonitrile, and water was tested, and the change in the weight of the membrane was measured as a function of time [48, 49].

As can be seen from Figs. 3(a)–3(c), the swelling of HOF membranes in water is higher than that of organic solvents, and the swelling is more serious in polar solvents and less in non-polar solvents, which is related to the hydrophilicity of the membranes. After swelling in water, the mass of HOF-TCPB membrane increased rapidly, and the growth rate gradually slowed down with time. After 30 days of immersion in water, the S_t increased to about 45%, whereas it stayed in the range of 30% for HOF@PEG and HOF@PVA membranes, reflecting the stability of the polyHOF membranes. This was attributed to the formation of hydrogen bonding of unbonded carboxylic acid groups after the introduction of the polymer, and the enhancement of the interlayer forces by electrostatic and π–π interactions, which inhibited the swelling of the membranes.

The FTIR spectra (Fig. S16 in the ESM) demonstrate that the hydrogen bonding network of HOF@PVA membranes did not undergo significant changes when immersed in solvents for 30 days, with the least relative decrease in peak intensity in the non-polar solvent. Meanwhile, being immersed in the solvent, the HOF@PEG hydroxyl feature peak did not show any significant

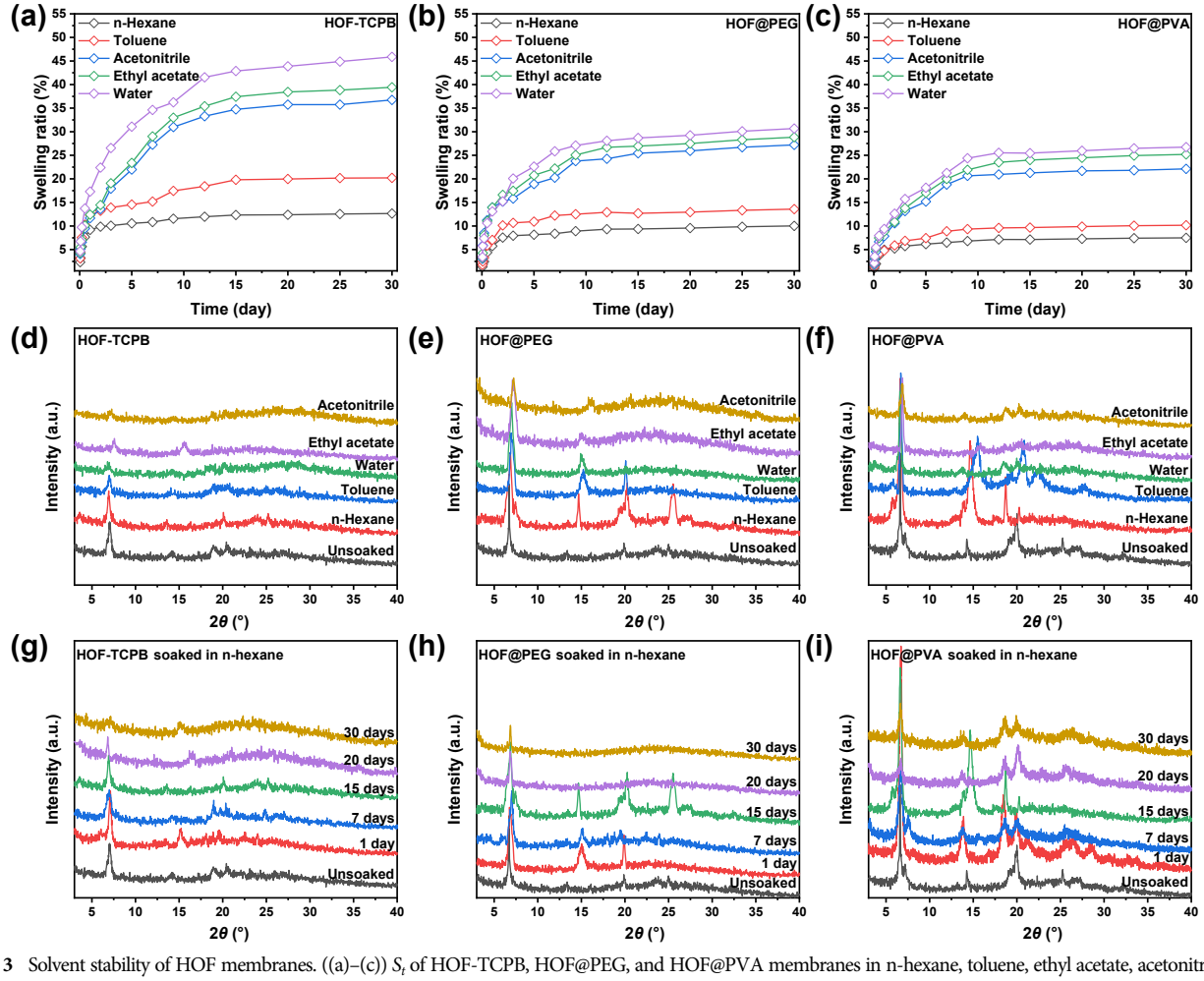

Figure 3 Solvent stability of HOF membranes. ((a)–(c)) S_t of HOF-TCPB, HOF@PEG, and HOF@PVA membranes in n-hexane, toluene, ethyl acetate, acetonitrile, and water for different time. ((d)–(f)) XRD patterns of HOF-TCPB, HOF@PEG, and HOF@PVA membranes in different organic solvents for 30 days. ((g)–(i)) XRD patterns of HOF-TCPB, HOF@PEG, and HOF@PVA after soaking in n-hexane for different time.

shifts, while the HOF-TCPB peak position was blue-shifted. The XRD patterns presented in Figs. 3(d)–3(f) demonstrate that the HOF@PVA lamellar membrane exhibits a slight displacement in the position and intensity of the typical peaks following 30 days of immersion in a range of solvents. In the non-polar solvent n-hexane, the position of the peak remains unaltered. However, in polar solvents, such as ethyl acetate and acetonitrile, the position and intensity of the typical peaks exhibit a slight change. The three HOF membranes were immersed in n-hexane in order to observe the evolution of the HOF membrane structure over time. As illustrated in Figs. 3(g)–3(i), the HOF@PVA membranes, when immersed in n-hexane for 30 days, exhibit no discernible shift in peak position. The position of the typical HOF@PEG peak remains unchanged while the intensity gradually decreases. HOF-TCPB membranes were immersed in n-hexane for 30 days, during which the typical peak gradually disappeared. These characteristics demonstrate that polyHOF membranes display favourable chemical stability [50].

In order to investigate the structural variation of the membranes in solvents, the membrane samples that had been soaked in solvents for different periods of time were characterized by SEM measurement. Figure 4 and Figs. S17–S20 in the ESM demonstrate the surface, cross-sectional morphologies, and optical photograph of the three HOF membranes after immersion in hexane, water, and acetonitrile, respectively. Generally, none of the membranes show micro-scale cracks among the nanosheet aggregates before solvent treatment. As immersion time increases, the cross-sectional morphologies of HOF-TCPB membranes change from crack-free to segregated lamellar in all types of solvents (Fig. S18 in the ESM), indicating that solvent molecules can easily enter the interlayer spacing of HOF-TCPB membranes and cause rather extent of swelling and crack generation. In particular, the HOF-TCPB membrane, after immersion in water or acetonitrile, showed significantly increased surface roughness (Fig. S17 in the ESM) and became almost exfoliated after soaking in water and polar solvents (Fig. S20 in the ESM). By comparison, after 30 days of solvent treatment, the morphologies of the two polyHOF membranes were better maintained for all the three solvents, indicative of good stability in solvents (Fig. 4 and Figs. S19 and S20 in the ESM). Nevertheless, as the most stable example in polyHOF membranes, HOF@PVA membranes show clearly enlarged content of phase segregation in acetonitrile, hinting that the membrane might suffer from instability in low-viscosity polar organic solvents.

To facilitate a more profound investigation into the mechanical behaviour of HOF membranes, we employed the nanoindentation technique. Upon comparing the three membranes, we observed distinct mechanical responses. The different elastic modulus (E) and hardness (H) values for HOF-TCPB (E = 0.31 GPa and H = 0.021 GPa), HOF@PEG (E = 0.45 GPa and H = 0.081 GPa), and HOF@PVA (E = 1.45 GPa and H = 0.120 GPa) in Fig. S21 in the ESM can be attributed to defects and interactions introduced during their self-assembly process. The polymer within the membranes restricts the movement of tips within them, resulting in steeper load-displacement curves, enhanced stiffness, and a higher elastic modulus. Consequently, these polyHOF membranes exhibit resistance to applied mechanical forces. Conversely, pristine HOF-TCPB nanosheets, which accumulate numerous defects, undergo considerable deformation under the same external force. As a result, the polyHOF membranes demonstrate greater fluidity during indentation loading, allowing the tip to move more freely within the membrane at lower stresses, thus ensuring flexibility. The mechanical properties of the composite membrane were quantified by analyzing the load–depth curves, as shown in Fig. S21 in the ESM. The HOF@PVA membranes exhibit excellent mechanical properties, with a higher tensile strength and flexibility than the original HOF-TCPB membrane. In the meantime, there was no significant change in mechanical strength of HOF@PVA membranes after immersion in solvents.

3.4 Solvent permeance and dye rejection

The effects of polymer type, polymer content and pressure on the separation performance were investigated. The dye rejection of HOF@PVA and HOF@PEG membranes is superior to that of HOF-TCPB membranes (Figs. 5(a) and 5(b)). Additionally, the polar solvent permeance of HOF@PVA membrane is greater than that of HOF@PEG membrane. This may be due to the formation of hydrogen bonds between the hydroxyl group of PVA and the unbonded carboxyl group of the HOF framework. Meanwhile, the water contact angle of HOF-TCPB is 69.5°, and the water contact angle of HOF@PVA membrane decreases to 27.8°, reflecting the increase in the hydrophilicity of the nanochannels (Fig. S22 in the ESM). The pressure cycling measurements indicate that HOF membranes show only a slight loss in water permeance when the pressure is adjusted from 1 to 5 bar and then returned to 1 bar (Fig. 5(c)). The water permeance of HOF-TCPB and HOF@PVA-x

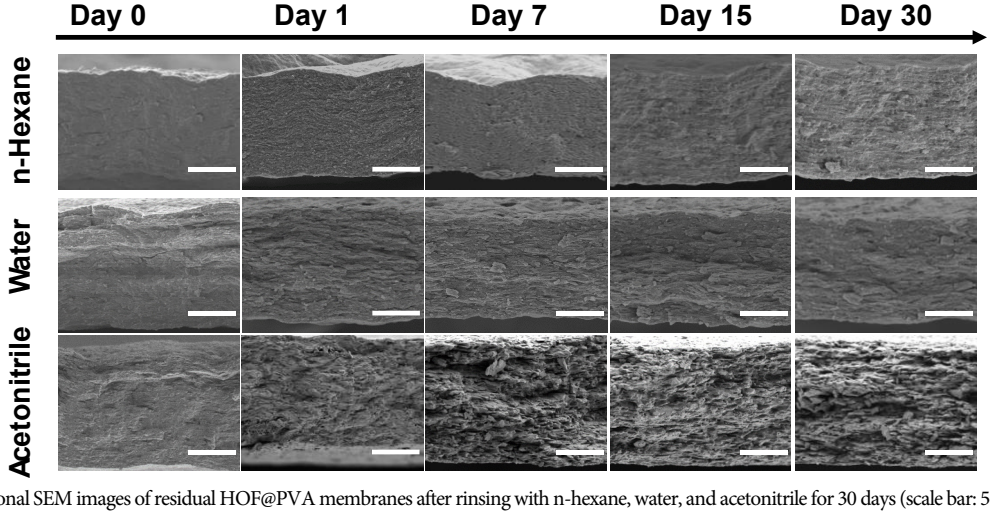

Figure 4 Cross-sectional SEM images of residual HOF@PVA membranes after rinsing with n-hexane, water, and acetonitrile for 30 days (scale bar: 5 μm).

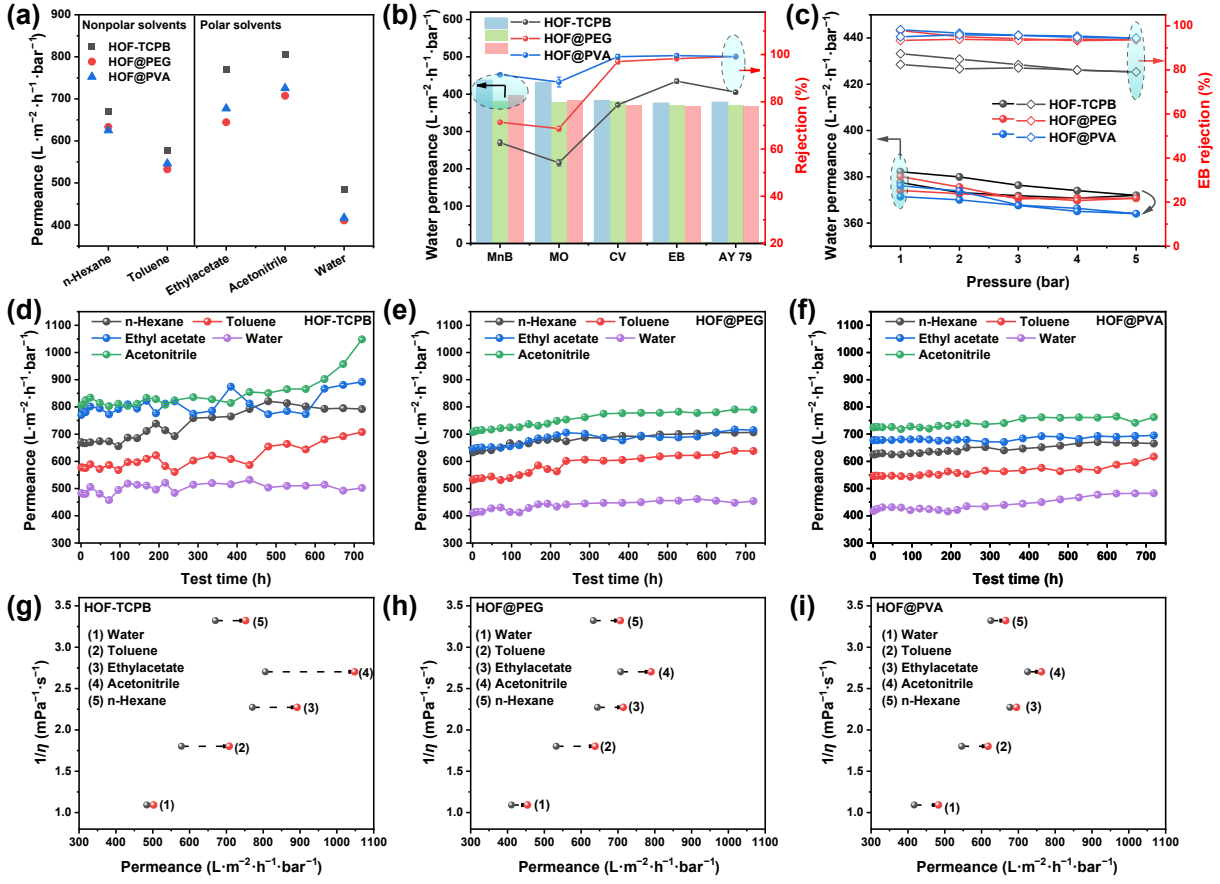

Figure 5 Nanofiltration permeance and long-term operation stability. (a) The permeance, (b) dye rejection, and (c) pressure cyclic measurement as a function of operation pressure of HOF-TCPB, HOF@PEG, and HOF@PVA membranes. ((d)–(f)) Long-term operation stability of HOF-TCPB, HOF@PEG, and HOF@PVA membranes in organic solvents for 720 h. ((g)–(i)) Change in solvent permeance before and after 30 days immersion of HOF-TCPB, HOF@PEG, and HOF@PVA membranes.

membranes with different PVA loadings (*x* refers to the mass ratio of PVA to HOF-TCPB nanosheets) were tested. Generally, the water permeance of membrane is inversely proportional to PVA loading since membrane thickness increases with it and thereby prolongs the solvent's diffusion pathway. Reducing thickness of membranes is an effective strategy to achieve high solvent permeance. However, the membranes might be too thin to guarantee defect-free surfaces and high selectivity. Figures S23(a) and S23(b) in the ESM illustrate a reduction in solvent permeance and significantly improve the dye rejection of the membranes following the addition of the polymer, but the excess content increases the mass transfer resistance and decreases the permeance of the membrane. The optimal HOF@PVA-0.3 membrane represents a satisfactory compromise between selectivity and solvent permeance (EB rejection > 99.6% and water permeance 367.8 $L{\cdot}m^{-2}{\cdot}h^{-1}{\cdot}bar^{-1}$). The effect of transmembrane pressure on the permeance of the HOF membranes was evaluated, as shown in Fig. S23(c) in the ESM. The water permeance of HOF@PVA-0.3 membrane decreases from 376.1 to 364.0 $L{\cdot}m^{-2}{\cdot}h^{-1}{\cdot}bar^{-1}$ from 1 to 5 bar. The pressure cycling measurements indicate that HOF membranes show only a slight loss in water permeance when the pressure is adjusted from 1 to 5 bar and then returned to 1 bar. During the ongoing separation process, the robust membrane maintains the integral membrane structure and demonstrates exceptional separation capabilities.

The time-dependent solvent permeance of HOF membranes after soaking in n-hexane for 30 days is shown in Figs. 5(d)–5(f). The performance stability of the separation membrane was assessed through long-term continuous operation. The results demonstrate that HOF@PVA membranes only have a slight decline of solvent permeance due to the membrane compaction, and then the permeance keeps almost unchanged with the long-term operating stability. As demonstrated in Figs. 5(g)–5(i), the permeance data of four solvents (except for n-hexane) after the long-term test appear consistent with the Poiseuille pore flow model, indicating that the membranes still possess typical porous structures and do not undergo excessive swelling. The exception observed for n-hexane may be related to its extremely low surface tension that hinders the dissolution on membrane surface. The polyHOF membranes also show excellent mechanical stability against bending or ultrasonication (Fig. S24 in the ESM), demonstrating the great promise they hold for further exploration.

4 Conclusion

This study reports a simple and effective synthesis strategy of polyHOF nanosheets by a hydrophilic polymer (PEG or PVA) for the preparation of 2D lamellar membranes. Thanks to the strong hydrogen bonding interactions between polymer chains and TCPB monomers, the introduced polymer contributes to the formation of highly crystalline frameworks rather than just physical blending with the original HOF-TCPB phase. More importantly, the PVA-introduced polyHOF nanosheets facilitate the creation of defect-free

membranes with greatly enhanced stability in water and organic solvents. Particularly, the crystalline structures of membranes are found to be well maintained after 30 days of immersion in both water and n-hexane, as well as the porous structures and rejection performance. These results demonstrate the prospects of fabrication of high-quality and stable polyHOF membranes for challenging applications involving liquid environment.

Electronic Supplementary Material: Supplementary material (SEM images, AFM images, and Raman spectroscopy measurements) is available in the online version of this article at https://doi.org/10.26599/NR.2025.94907406.

Data availability

All data needed to support the conclusions in the paper are presented in the manuscript and the Electronic Supplementary Material. Additional data related to this paper may be requested from the corresponding author upon request.

Acknowledgements

The authors gratefully acknowledge the financial support for this research by National Key R&D Program of China (Nos. 2022YFB3805204 and 2022YFB3805202) and the Key Science and Technology Project of Henan Province (No. 242102321032). We also gratefully acknowledge the instrument support from Center of Advanced Analysis & Computational Science, Zhengzhou University.

Declaration of competing interest

All the contributing authors report no conflict of interests in this work.

Author contribution statement

J. J. D.: Investigation, data curation, formal analysis, writing – original draft. X. W. : Formal analysis, data curation. W. L. L: Investigation, formal analysis. J. J. C.: Investigation, methodology, formal analysis. R. L. L.: Investigation, formal analysis. X. L. W.: Writing – review and editing, validation. Y. N. L.: Funding acquisition, Project administration, Resources. W. J. W.: Supervision, visualization. Y. F. L.: Writing – review & editing, validation, project administration. J. T. W.: Writing – review & editing, project administration, funding acquisition. All the authors have approved the final manuscript.

Use of AI statement

None.

References

[1] Xiao, H.; Feng, Y. Y.; Goundry, W. R. F.; Karlsson, S. Organic solvent nanofiltration in pharmaceutical applications. *Org. Process Res. Dev.* **2024**, *28*, 891–923.

[2] Sholl, D. S.; Lively, R. P. Seven chemical separations to change the world. *Nature* **2016**, *532*, 435–437.

[3] Marquardt, T.; Lüning, U. Towards golf ball shaped reagents: Dendrimer fixed concave pyridines. *Chem. Commun.* **1997**, 1681–1682.

[4] Sirkar, K. K. Application of membrane technologies in the pharmaceutical industry. *Curr. Opin. Drug. Discov. Dev.* **2000**, *3*, 714–722.

[5] Van Der Bruggen, B.; Vandecasteele, C.; Van Gestel, T.; Doyen, W.; Leysen, R. A review of pressure-driven membrane processes in wastewater treatment and drinking water production. *Environ. Prog.* **2003**, *22*, 46–56.

[6] Wang, Z. G.; Luo, X. F.; Zhang, J. Q.; Zhang, F.; Fang, W. X.; Jin, J. Polymer membranes for organic solvent nanofiltration: Recent progress, challenges and perspectives. *Adv. Membr.* **2023**, *3*, 100063.

[7] Ma, Q.; Li, J. J.; Li, Y. S.; Choi, J. Recent progress and issues facing zeolite and metal–organic framework membranes: From membrane synthesis to applications. *J. Membr. Sci.* **2024**, *690*, 122201.

[8] Jones, C. W. Metal–organic frameworks and covalent organic frameworks: Emerging advances and applications. *JACS Au* **2022**, *2*, 1504–1505.

[9] Jaid, G. M.; AbdulRazak, A. A.; Meskher, H.; Al-Saadi, S.; Alsalhy, Q. F. Metal–organic frameworks (MOFs), covalent organic frameworks (COFs), and hydrogen-bonded organic frameworks (HOFs) in mixed matrix membranes. *Mater. Today Sustain.* **2024**, *25*, 100672.

[10] Bai, W.; Wang, F.; Yan, L. J.; Sun, H. X.; Zhu, Z. Q.; Chen, L. H.; Li, J. Y.; Liang, W. D.; Li, A. Porous organic polymers (POPs) membrane via thiol-yne click chemistry for efficient particulate matter capture and microplastics separation. *Microporous Mesoporous Mat.* **2022**, *329*, 111509.

[11] Lu, Y. Q.; Liu, W.; Liu, J. T.; Li, X.; Zhang, S. A review on 2D porous organic polymers for membrane-based separations: Processing and engineering of transport channels. *Adv. Membr.* **2021**, *1*, 100014.

[12] Pan, Y. C.; Li, T.; Lestari, G.; Lai, Z. P. Effective separation of propylene/propane binary mixtures by ZIF-8 membranes. *J. Membr. Sci.* **2012**, *390*, 93–98.

[13] Li, P. H.; Ryder, M. R.; Stoddart, J. F. Hydrogen-bonded organic frameworks: A rising class of porous molecular materials. *Acc. Mater. Res.* **2020**, *1*, 77–87.

[14] Karmakar, A.; Illathvalappil, R.; Anothumakkool, B.; Sen, A.; Samanta, P.; Desai, A. V.; Kurungot, S.; Ghosh, S. K. Hydrogen-bonded organic frameworks (HOFs): A new class of porous crystalline proton-conducting materials. *Angew. Chem., Int. Ed.* **2016**, *55*, 10667–10671.

[15] Huang, Q. Y.; Chen, X. X.; Li, W. L.; Yang, Z. Y.; Zhang, Y.; Zhao, J.; Chi, Z. G. Local dynamics in a hydrogen-bonded organic framework for adaptive guest accommodation with programmable luminescence. *Chem* **2023**, *9*, 1241–1254.

[16] Mohan, B.; Singh, G.; Gupta, R. K.; Sharma, P. K.; Solovev, A. A.; Pombeiro, A. J. L.; Ren, P. Hydrogen-bonded organic frameworks (HOFs): Multifunctional material on analytical monitoring. *TrAC Trends Analyt. Chem.* **2024**, *170*, 117436.

[17] Hisaki, I.; Xin, C.; Takahashi, K.; Nakamura, T. Designing hydrogen-bonded organic frameworks (HOFs) with permanent porosity. *Angew. Chem., Int. Ed.* **2019**, *58*, 11160–11170.

[18] Li, Z. W.; Huang, Z. J.; Li, Y. X.; Wu, X. M.; Shi, W.; Zhang, Y. B.; Ma, X. M.; Ouyang, G. F.; Ye, B. H.; Liu, G. F. et al. An ultrastable, easily scalable and regenerable macrocycle-based hydrogen-bonded organic framework. *CCS Chem.* **2025**, *7*, 293–306.

[19] Feng, J. F.; Liu, T. F.; Cao, R. An electrochromic hydrogen-bonded organic framework film. *Angew. Chem., Int. Ed.* **2020**, *59*, 22392–22396.

[20] Zhang, A. A.; Li, Y. L.; Fang, Z. B.; Xie, L.; Cao, R.; Liu, Y. Y.; Liu, T. F. Facile preparation of hydrogen-bonded organic framework/Cu_2O heterostructure films via electrophoretic deposition for efficient CO_2 photoreduction. *ACS Appl. Mater. Interfaces* **2022**, *14*, 21050–21058.

[21] Li, W.; Li, Y. H.; Caro, J.; Huang, A. S. Fabrication of a flexible hydrogen-bonded organic framework based mixed matrix membrane for hydrogen separation. *J. Membr. Sci.* **2022**, *643*, 120021.

[22] Kang, L. L.; Zuo, S. W.; Han, B. X.; Li, G. Comparative study on proton conductivity of a polypyridinyl multicarboxylate-based hydrogen-bonded organic framework and related chitosan composite membrane. *New J. Chem.* **2023**, *47*, 1299–1307.
[23] Yang, Z. W.; Zhang, Y. F.; Wu, W. J.; Zhou, Z. F.; Gao, H. X.; Wang, J. T.; Jiang, Z. Y. Hydrogen-bonded organic framework membrane with efficient proton conduction. *J. Membr. Sci.* **2022**, *664*, 121118.
[24] Wang, B.; Lin, R. B.; Zhang, Z. J.; Xiang, S. C.; Chen, B. L. Hydrogen-bonded organic frameworks as a tunable platform for functional materials. *J. Am. Chem. Soc.* **2020**, *142*, 14399–14416.
[25] Liu, B. T.; Pan, X. H.; Nie, D. Y.; Hu, X. J.; Liu, E. P.; Liu, T. F. Ionic hydrogen-bonded organic frameworks for ion-responsive antimicrobial membranes. *Adv. Mater.* **2022**, *34*, 2202280.
[26] Yang, Z. B.; Li, D. D.; Ao, D.; Ma, C.; Li, N.; Sun, Y. X.; Qiao, Z. H.; Zhong, C. L.; Guiver, M. D. Self-supported membranes fabricated by a polymer-hydrogen bonded network with a rigidified MOF framework. *J. Membr. Sci.* **2022**, *650*, 120427.
[27] Zhang, Z. J.; Nguyen, H. T. H.; Miller, S. A.; Cohen, S. M. polyMOFs: A class of interconvertible polymer-metal–organic framework hybrid materials. *Angew. Chem., Int. Ed.* **2015**, *54*, 6152–6157.
[28] Hisaki, I.; Affendy, N. Q. E.; Tohnai, N. Precise elucidations of stacking manners of hydrogen-bonded two-dimensional organic frameworks composed of X-shaped π-conjugated systems. *CrystEngComm* **2017**, *19*, 4892–4898.
[29] Hisaki, I.; Nakagawa, S.; Ikenaka, N.; Imamura, Y.; Katouda, M.; Tashiro, M.; Tsuchida, H.; Ogoshi, T.; Sato, H.; Tohnai, N. et al. A series of layered assemblies of hydrogen-bonded, hexagonal networks of C_3-symmetric π-conjugated molecules: A potential motif of porous organic materials. *J. Am. Chem. Soc.* **2016**, *138*, 6617–6628.
[30] Yu, D. H.; Sun, L. Y.; Zhang, Y. N.; Song, Y.; Jia, C. Y.; Wang, Y.; Wang, Y. X.; Kipper, M. J.; Tang, J. G.; Huang, L. J. Two-dimensional graphene oxide/MXene lamellar membrane cross-linked by urea with adjustable interlayer spacing for efficient dye rejection and ion sieving. *Chem. Eng. J.* **2024**, *480*, 148009.
[31] Zhao, Y. Y.; Tong, X.; Kim, J.; Tong, T. Z.; Huang, C. H.; Chen, Y. S. Capillary-assisted fabrication of thin-film nanocomposite membranes for improved solute-solute separation. *Environ. Sci. Technol.* **2022**, *56*, 5849–5859.
[32] Zhang, H.; Li, X. Y.; Xu, T. W. Two-dimensional graphene oxide nanochannel membranes for ionic separation. *Curr. Opin. Chem. Eng.* **2023**, *39*, 100899.
[33] Rodenas, T.; Luz, I.; Prieto, G.; Seoane, B.; Miro, H.; Corma, A.; Kapteijn, F.; Llabrés I Xamena, F. X.; Gascon, J. Metal–organic framework nanosheets in polymer composite materials for gas separation. *Nat. Mater.* **2015**, *14*, 48–55.
[34] Ghosh, A.; Moulder, J.; Bröring, M.; Vogel, E. X-ray photoelectron spectroscopy of porphycenes: Charge asymmetry across low-barrier hydrogen bonds. *Angew. Chem., Int. Ed.* **2001**, *40*, 431–434.
[35] Zhang, G. L.; Tang, K. J.; Zhang, X.; Xu, L. S.; Shen, C.; Meng, Q. Self-assembly of defect-free polymer-based zeolite imidazolate framework composite membranes with metal-phenolic networks for high efficient H_2/CH_4 separation. *J. Membr. Sci.* **2021**, *617*, 118612.
[36] Li, Y. F.; Jia, H. P.; Cheng, Q. L.; Pan, F. S.; Jiang, Z. Y. Sodium alginate–gelatin polyelectrolyte complex membranes with both high water vapor permeance and high permselectivity. *J. Membr. Sci.* **2011**, *375*, 304–312.
[37] Kolesov, B. A. Hydrogen bonds: Raman spectroscopic study. *Int. J. Mol. Sci.* **2021**, *22*, 5380.
[38] Kolesov, B. A. A Raman spectroscopy study of tautomeric O–H···O hydrogen bonding. *J. Struct. Chem.* **2020**, *61*, 1186–1194.
[39] Du, M. X.; Yuan, Y. F.; Zhang, J. M.; Liu, J. J.; Liu, C. Y. Polymer solubility mechanism in ionic liquids: ^{1}H NMR spectra and two-parameter hydrogen bonding analysis. *Phys. Chem. Chem. Phys.* **2024**, *26*, 16942–16946.
[40] Wang, F. F.; Wang, P.; Niu, H. Y.; Yu, Y. F.; Sun, P. C. Solid-state NMR studies on hydrogen bonding interactions and structural evolution in PAA/PEO blends. *Acta Phys. Chim. Sin.* **2020**, *36*, 1912016.
[41] Jiang, S.; Qiao, C. D.; Liu, R. P.; Liu, Q. Z.; Xu, J.; Yao, J. S. Structure and properties of citric acid cross-linked chitosan/poly(vinyl alcohol) composite films for food packaging applications. *Carbohydr. Polym.* **2023**, *312*, 120842.
[42] O'Shea, J. N.; Schnadt, J.; Brühwiler, P. A.; Hillesheimer, H.; Mårtensson, N.; Patthey, L.; Krempasky, J.; Wang, C. K.; Luo, Y.; Ågren, H. Hydrogen-bond induced surface core-level shift in isonicotinic acid. *J. Phys. Chem. B* **2001**, *105*, 1917–1920.
[43] Liu, R.; Li, W. H. High-thermal-stability and high-thermal-conductivity $Ti_3C_2T_x$ MXene/poly(vinyl alcohol) (PVA) composites. *ACS Omega* **2018**, *3*, 2609–2617.
[44] Pires, J. Simultaneous thermogravimetry-differential scanning calorimetry (TG-DSC) in nanoporous materials: Examples of data for zeolites, metal–organic frameworks (MOFs), clay based and mesostructured solids. *J. Inorg. Organomet. Polym. Mater.* **2024**, *34*, 3346–3359.
[45] Yang, D.; Chen, Y. Y.; Cao, L. H. High proton conductivity of sulfonate-amine ionic HOFs and enhancement of SPEEK composite membranes. *Chem.—Asian J.* **2024**, *19*, e202400870.
[46] Song, X. Y.; Wang, C.; Gao, X. Y.; Wang, Y.; Xu, R.; Wang, J.; Li, P. Thermally crosslinked hydrogen-bonded organic framework membranes for highly selective ion separation. *Molecules* **2023**, *28*, 2173.
[47] Gao, H. X.; Gao, Z. P.; Ye, C.; Zhou, G. L.; Yang, Z. W.; Dai, K.; Wu, W. J.; Wang, J. T. Free-standing polymer-metal–organic framework membrane with high proton conductivity and water stability. *Nano Res.* **2023**, *16*, 7950–7957.
[48] Zhong, D. L.; Wang, Z. G.; Lan, Q. Q.; Wang, Y. Selective swelling of block copolymer ultrafiltration membranes for enhanced water permeability and fouling resistance. *J. Membr. Sci.* **2018**, *558*, 106–112.
[49] Suleman, M. S.; Lau, K. K.; Yeong, Y. F. Enhanced gas separation performance of PSF membrane after modification to PSF/PDMS composite membrane in CO_2/CH_4 separation. *J. Appl. Polym. Sci.* **2018**, *135*, 45650.
[50] Ma, K. K.; Li, P.; Xin, J. H.; Chen, Y. W.; Chen, Z. J.; Goswami, S.; Liu, X. F.; Kato, S.; Chen, H. Y.; Zhang, X. et al. Ultrastable mesoporous hydrogen-bonded organic framework-based fiber composites toward mustard gas detoxification. *Cell. Rep. Phys. Sci.* **2020**, *1*, 100024.